The impact of turbulence processes on ionospheric plasma density irregularities

Paola De Michelis, I. Coco, G. Consolini, F. Giannattasio, G. Lovati, M. Pezzopane, A. Pignalberi and R. Tozzi

3rd URSI AT-AP-RASC, Gran Canaria, 29 May - 3 June 2022

Aim

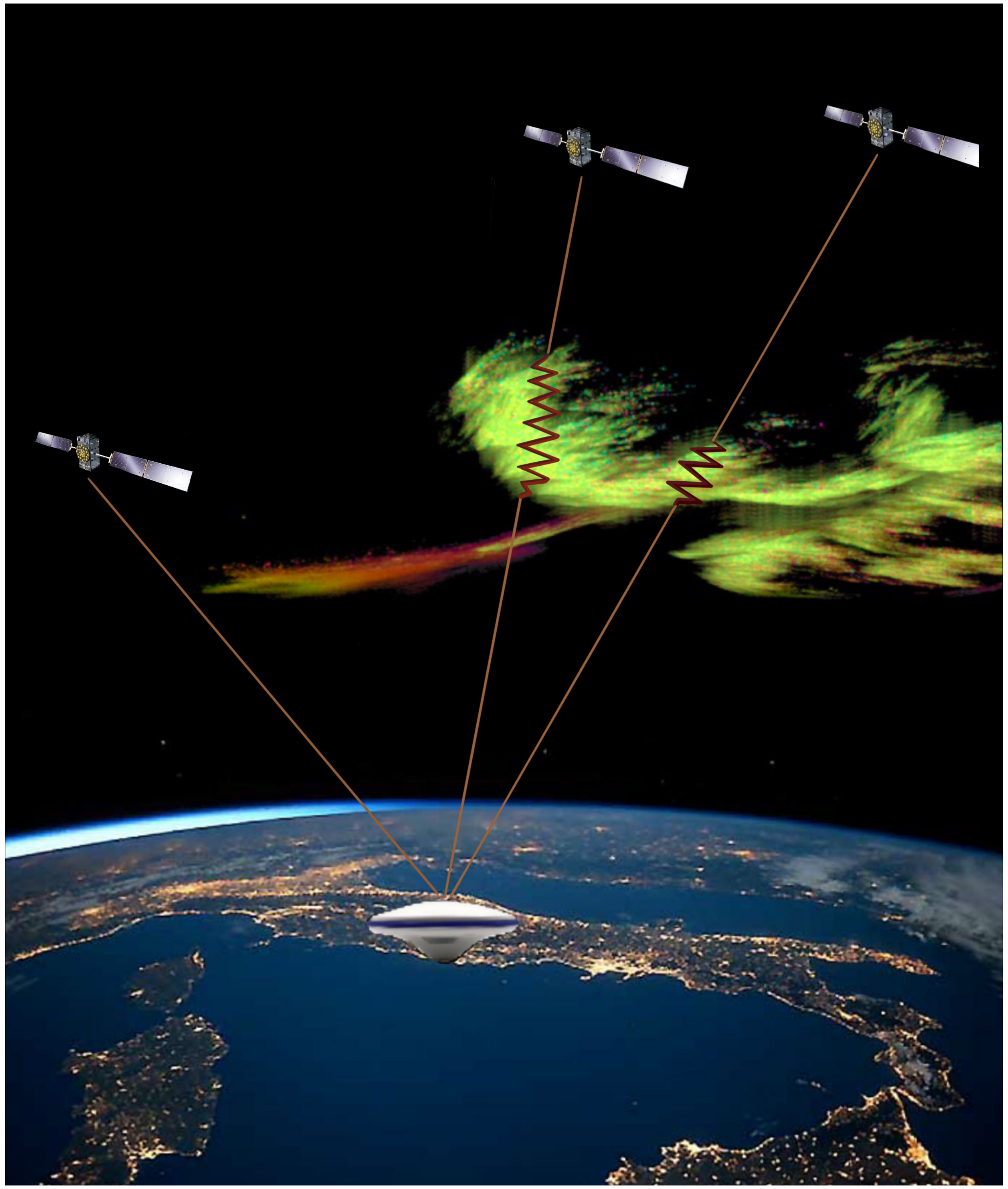

We used data recorded onboard of Swarm constellation

- to better understand the plasma density irregularities
- to investigate their possible turbulent nature
- to assess the possible dependence of the GPS signals loss of lock on the presence of a specific kind of ionospheric irregularities and thereby appraise the origin of one of the largest space weather effects on the GNSS systems and users.

Introduction

There is a growing body of literature that recognizes the importance of **the intermittent turbulent phenomena** in the ionospheric environment.

Fluctuations of **plasma density, electrostatic potential and magnetic and electric fields** have highlighted the existence of a turbulent state in the ionosphere.

This state, which can be detected at different spatial scales, plays a fundamental role in the overall ionospheric dynamics.

Capture the role of Turbulence in the ionosphere

It is able to generate/create magnetic and plasma structures that can strongly affect the homogeneity of the plasma in the ionospheric regions.

For example turbulence has been claimed to explain the upwelling propagation of the **Equatorial Plasma Bubbles.** These are ionospheric plasma depletions generated by electrostatic Rayleigh-Taylor instability.

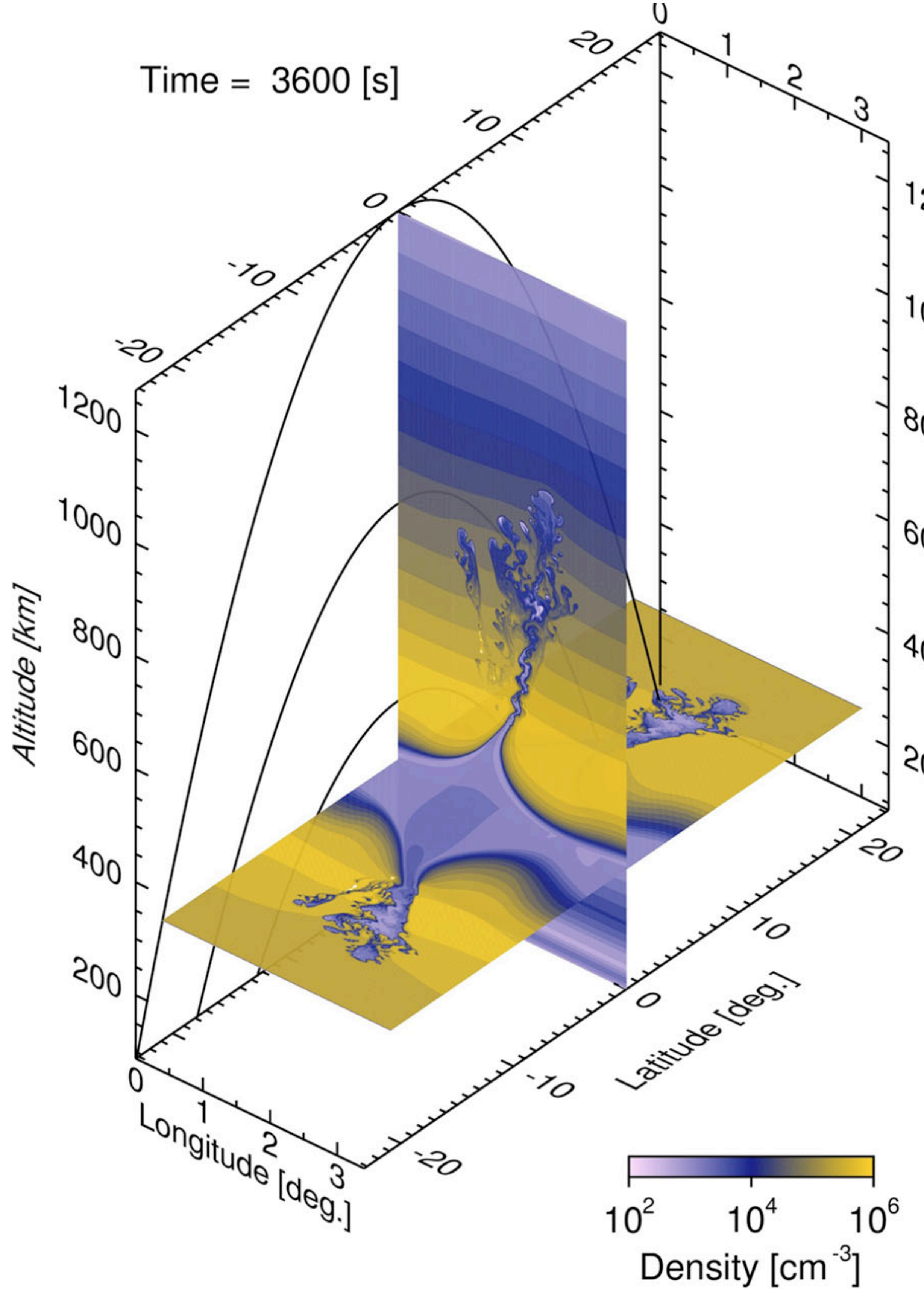

Yokoyama, Progress in Earth and Planetary Science , 37, 2017

Introduction

Not all the plasma density variations have a turbulent origin.

It is known that ionospheric irregularities can affect the propagation of radio signals that pass through the ionosphere or are reflected by it.

One example of these effects is the loss of lock (LoL) and range errors in Global Navigation Satellite System (GNSS).

LoL is a condition for which a GNSS receiver can no longer track the signal sent by the satellite.

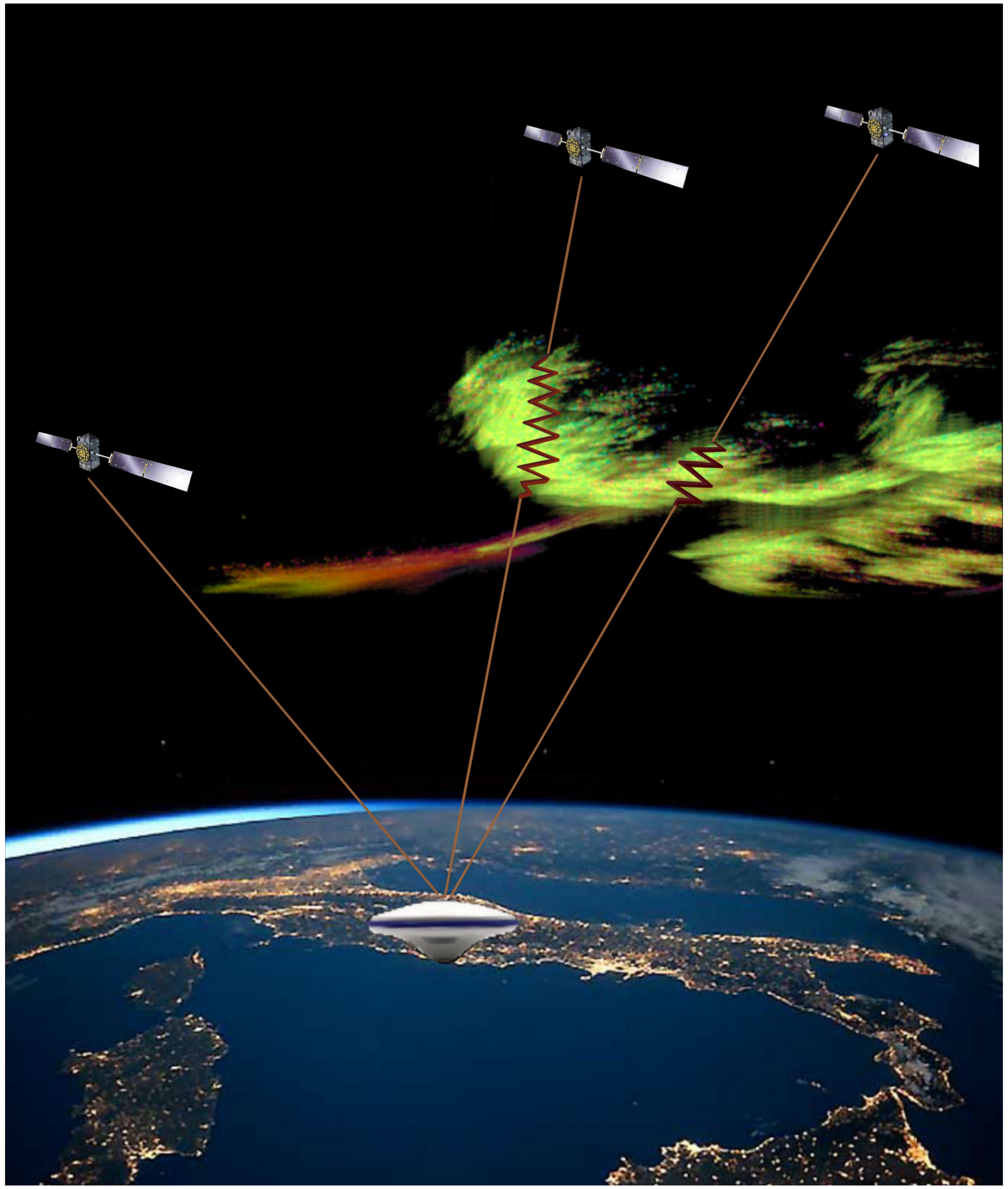

Introduction

In our society Global Navigation Satellite Systems are fundamental. Critical infrastructures, such as power systems, railway control, civil and military aviation, government services and so on depend on the proper functioning of these systems.

Understanding the sources of the ionospheric density variability and monitoring its dynamics during space rather events is of great practical importance.

Data

★ We used data recorded onboard Swarm constellation. It consists of three identical satellites named Alpha, Bravo, and Charlie (A, B and C); which were launched on 22 November 2013 into a near-polar orbit.

★Swarm A and C form the lower pair of satellites flying side-by-side at an altitude of 462 km (initial altitude) and at 87.35° inclination angle, whereas Swarm B is cruising at a higher orbit of 511 km (initial altitude) and at 87.75° inclination angle.

★All the three Swarm satellites are equipped with the same set of identical instruments.

Data

★ We used data recorded onboard Swarm constellation. It consists of three identical satellites named Alpha, Bravo, and Charlie (A, B and C); which were launched on 22 November 201

★Swarm A and
satellites flying
462 km (initial
inclination angl
cruising at a hi
altitude) and at

★All the three Swarm satellite are equipped with the same set of identical instruments.

Swarm A & Swarm B
15 July 2014 - 31 December 2021

Data

★ 1Hz **Electron density** (Ne) time series.

★ **RODI** (Rate of Change of electron density index) with 1s time resolution. RODI is the standard deviation of Ne time derivative calculated on a window of fixed width ($\Delta t = 10s$) sliding along Ne time series.

★**Loss of Lock** time series. The LoL events are identified by looking for interruptions in the sTEC time series for a specific GPS satellite, which is identified by the corresponding Pseudo Random Noise number (PRN).

Data

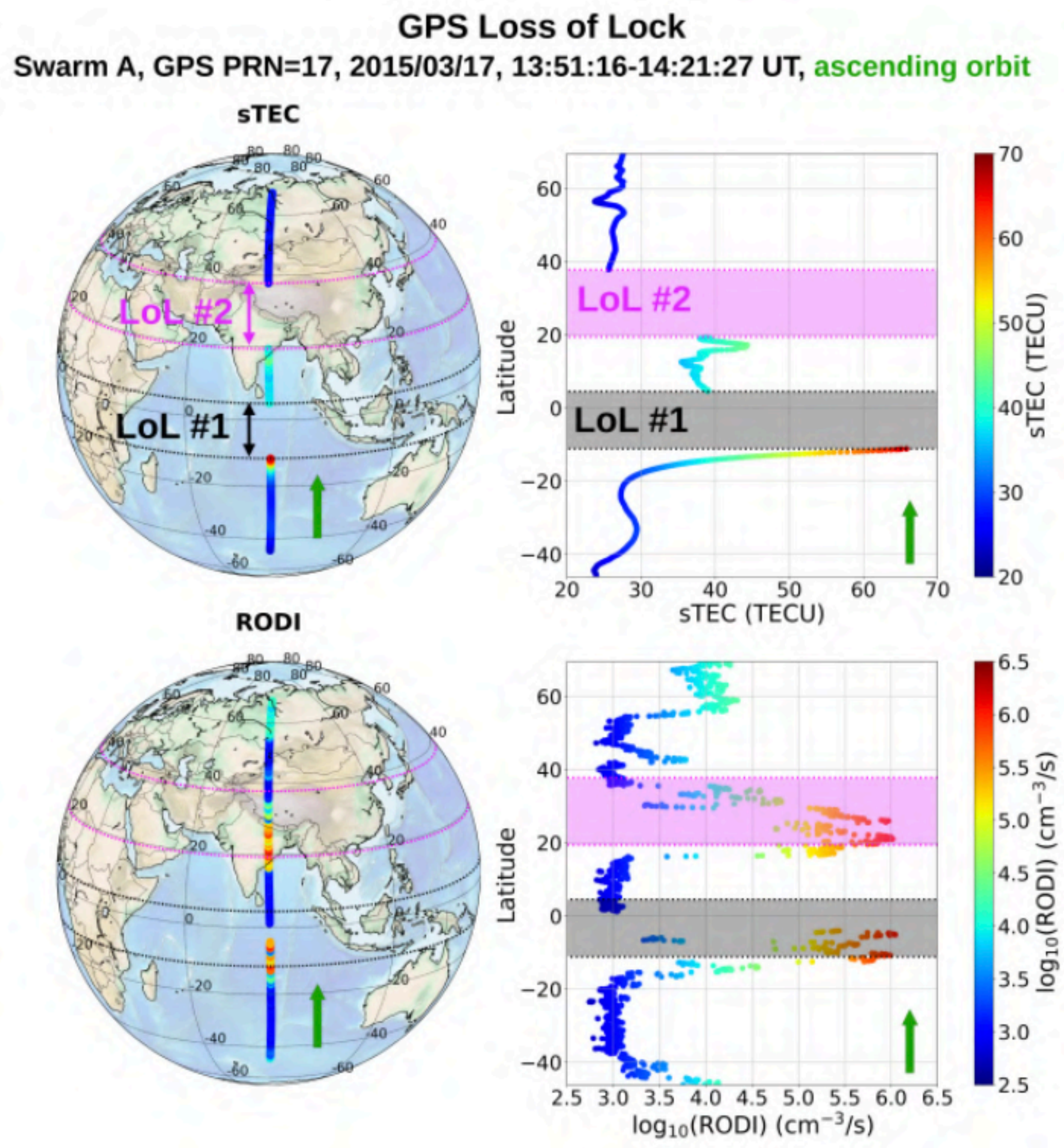

Example of GPS LoL events as identified in the sTEC time series measured by Swarm A during an orbit and corresponding RODI values calculated from Ne measurements.

The magenta and grey belts identify the GPS LoL duration.

Left panels represent the satellite track in a geographic coordinates map, while the right panels show the corresponding plot latitude vs value (sTEC or RODI).

Method of Analysis: Structure Functions

We consider **qth-order structure function** $S_q(\tau)$, which for a signal $N_e(t)$ defined over an interval T is given by

$$S_q(\tau) =< |N_e(t+\tau) - N_e(t)|^q >_T$$

when we deal with a scale-invariant signal the $S_q(\tau)$ exhibits a power law behavior:

$$S_q(\tau) \sim \tau^{\gamma(q)}$$

We have estimated:

$\gamma(1)$ first-order scaling exponent, known as Hurst exponent

$\gamma(2)$ second-order scaling exponent, which provides the **Fourier power spectral density exponent** β through Wiener-Khinchin theorem ($\beta = \gamma(2) + 1$)

Method of Analysis: Structure Functions

$$S_1(\tau) = <|N_e(t+\tau) - N_e(t)|>_T \sim \tau^{\gamma(1)}$$

The estimation of the scaling features is done for Ne fluctuations at timescales smaller than 40 s, using a moving window of T=400 s. The Ne fluctuations in the range from 1 s to 40 s correspond to investigation of **spatial fluctuations from 7.6 km up to 300 km**. The choice of a moving window of 400 s, which is 10 times larger than the maximum scale which we want to investigate (40 s), permits us to have a reliable estimation of 40 s fluctuation statistics.

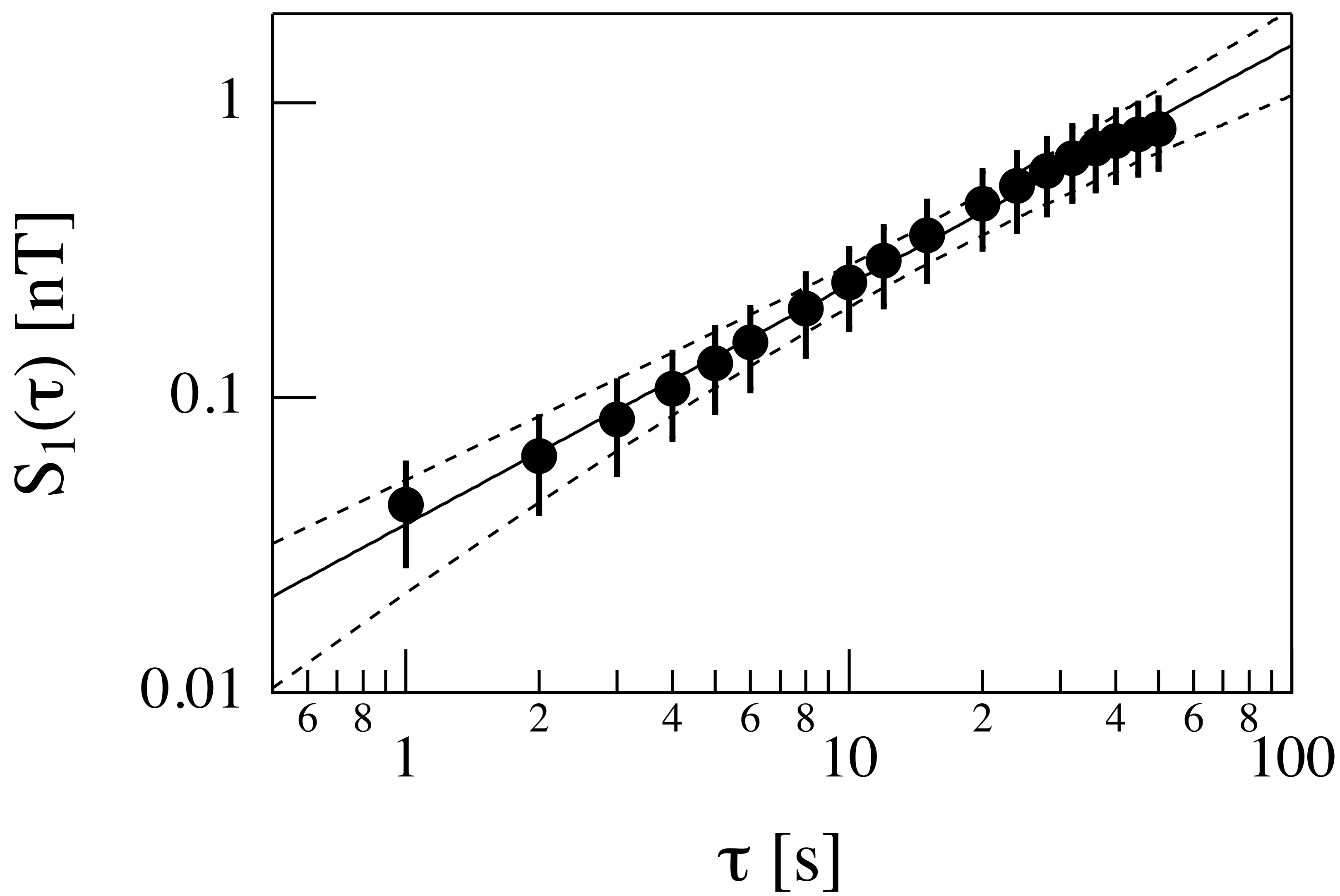

We are looking at MESO-SCALE

Scaling Exponents in Brief: Meaning

$\gamma(1)$=H

Provides information on the range of correlation of the investigated quantity: values of **H<0.5** are the evidence of the **anti-persistent character** of its increments so that we can talk of short correlated signals, values of **H>0.5** are the evidence of the **persistent character** of its increments so that we can talk of long-range correlated signals.

$$\gamma(2) = \beta - 1$$

Through $\beta = \gamma(2)+1$ provides information on the spectral features of the quantity under investigation, representing the slope of a power law PSD can provide information on the presence of turbulence.

Results: Mid and High Latitude (|QDLat|>50°)

We identify two distinct classes of plasma density fluctuations in the ionosphere which are characterized by different values of both the scaling exponents and RODI.

- **Low values of RODI** are mainly associated with Ne fluctuations characterized by a persistent ($\gamma(1) > 0.5$) behavior and a second-order scaling exponent $\gamma(2)>1$.

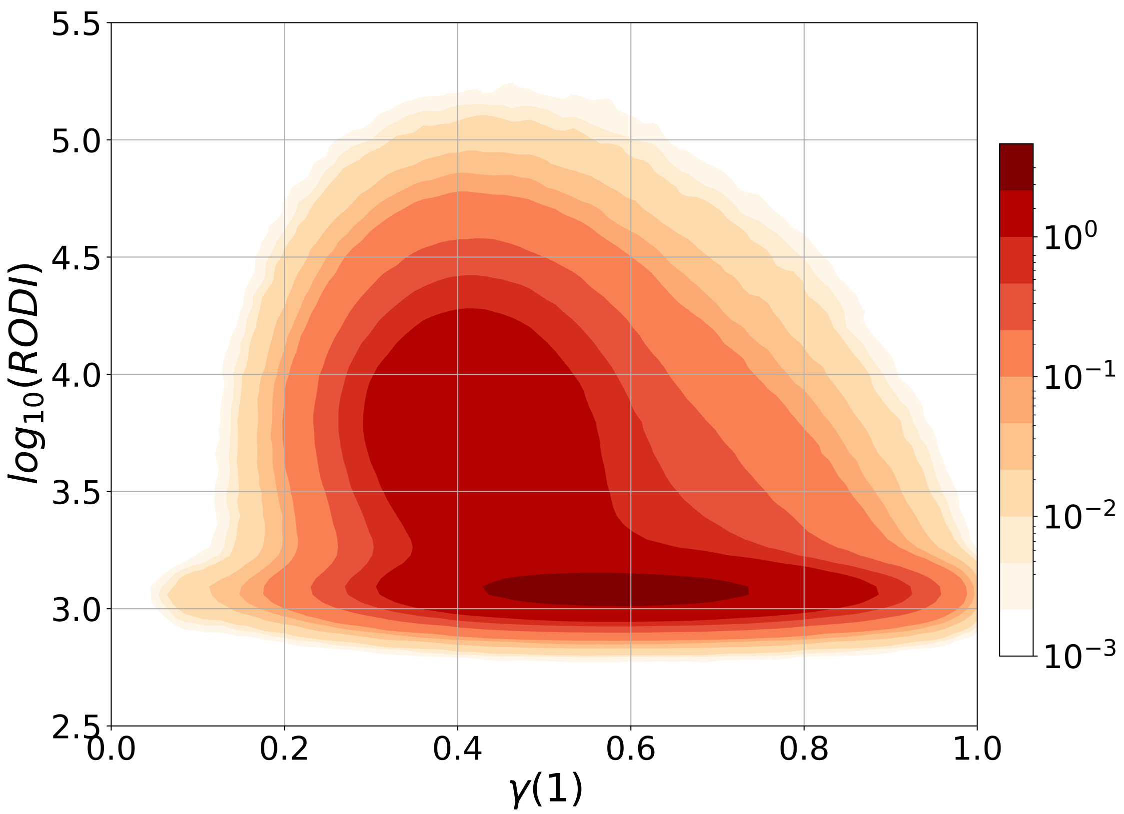

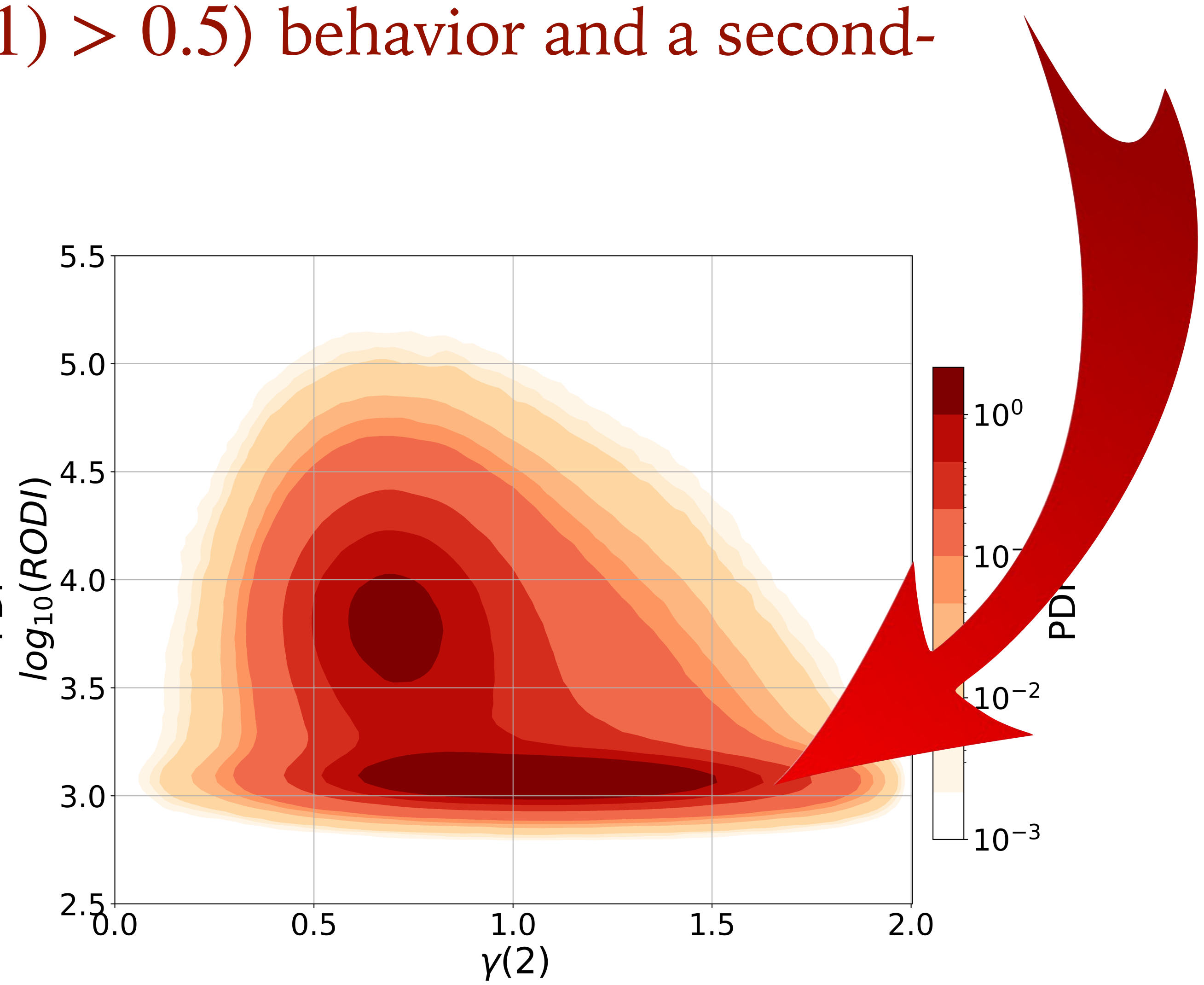

Results: Mid and High Latitude (|QDLat|>50°)

We identify two distinct classes of plasma density fluctuations in the ionosphere which are characterized by different values of both the scaling exponents and RODI.

- **High values of RODI** are generally associated with Ne fluctuations characterized by an antipersistent ($\gamma(1) < 0.5$) behavior and a second-order scaling exponent $\gamma(2) < 1$.

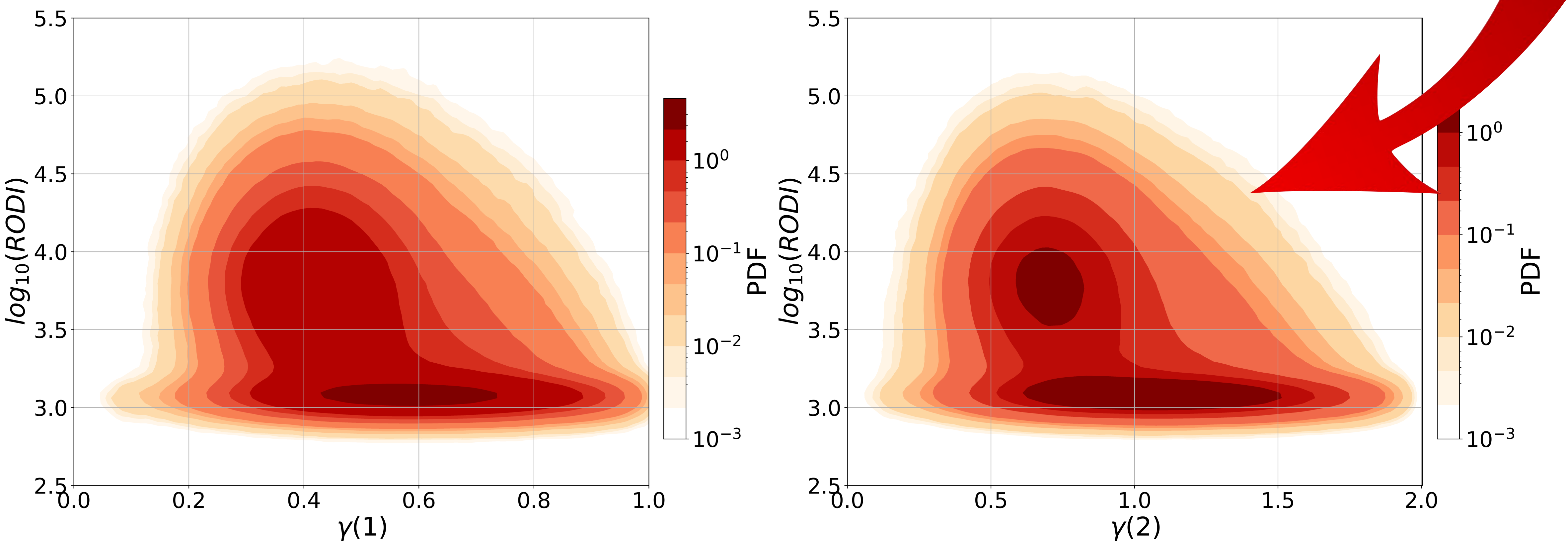

Results: Mid and High Latitude (QDLat>50°)

- The **class characterized by antipersistency, $\gamma(2) < 1$ and high values of RODI**) is mainly located at high latitude inside the auroral oval and the polar cap. These scaling exponent values are compatible with some processes that generally occur at high latitudes as the **gradient-drift/current convective instability** and the **Kelvin-Helmholtz instability**.

- The **class characterized by persistency, $\gamma(2) > 1$ and low values of RODI**, is located at lower latitudes, mainly outside the auroral oval.

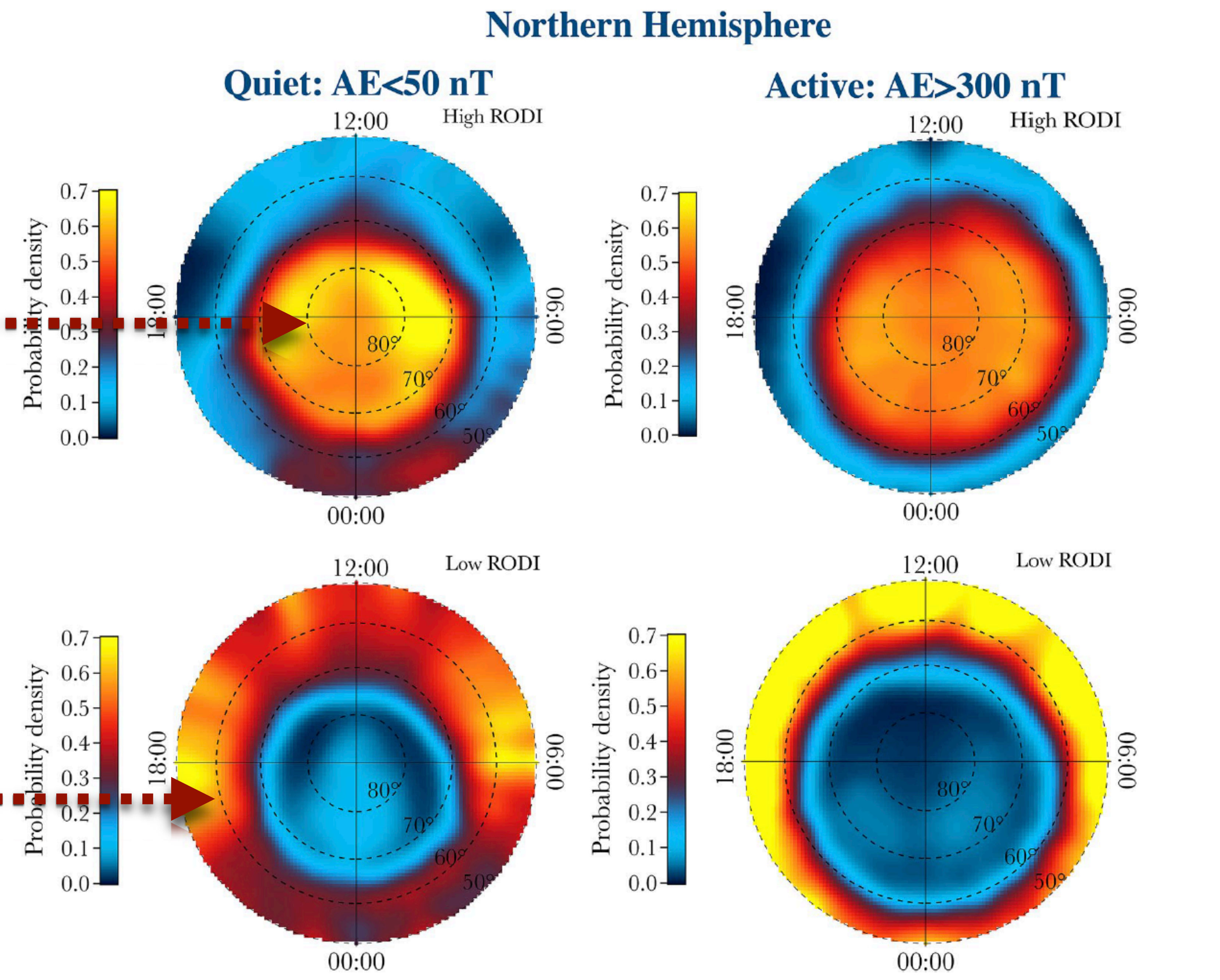

Distributions of the probability densities of the two families in the QDLat–MLT plane associated with high (top panels) and low (bottom panels) values of RODI in the Northern Hemisphere for quiet and active periods, respectively.

Results: Mid and High Latitude (QDLat>50°)

Once LoL events have been identified in time and space, it is possible to investigate the features of the ionospheric environment that favor their occurrence.

We consider all the LoL events and analyze the corresponding local fluctuation scaling properties of the Ne measurements, which are essential to understand and characterize the complexity of the structure.

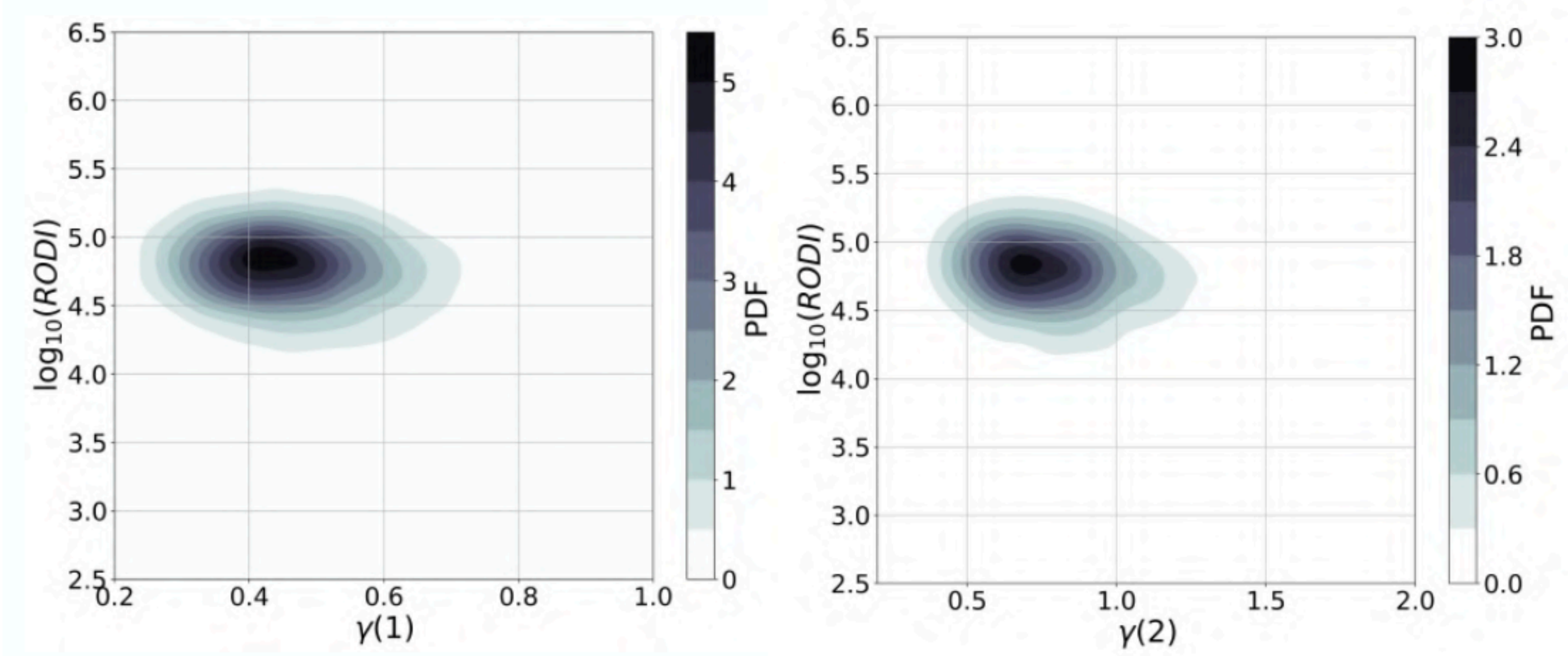

Conditioned joint PDF of RODI and $\gamma(1)$ and $\gamma(2)$ for the joint dataset (Swarm A + Swarm B). Data refer to mid and high latitudes (**|QDLat|>50°**) and are those calculated simultaneously to the occurrence of GPS LoL events.

Results: Mid and High Latitude (QDLat>50°)

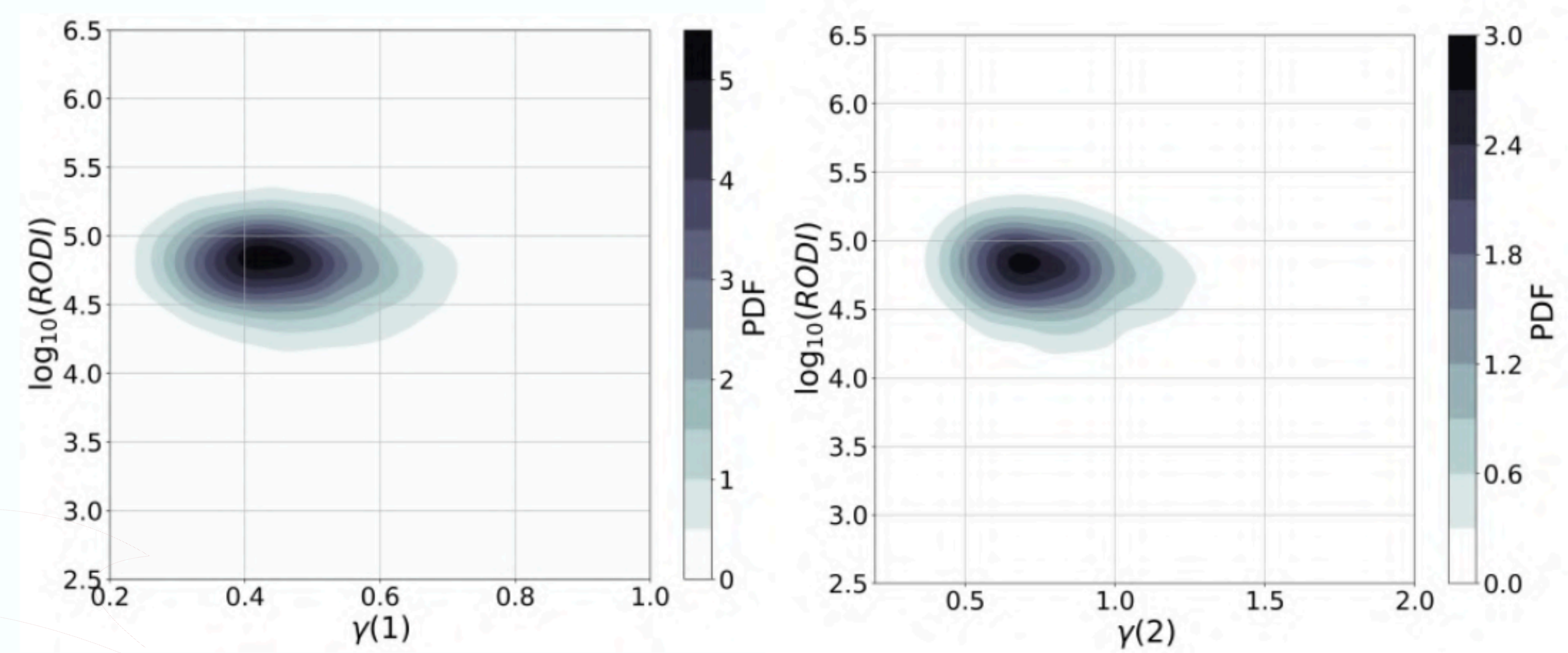

GPS LoL events are mainly associated with $\gamma(1) = (0.47 \pm 0.12)$

Ne fluctuations during LoL events have an anti-persistent character, i.e., there is not a long-term memory effects on the fluctuations sign.

Results: Mid and High Latitude (QDLat>50°)

GPS LoL events are mainly associated with $\gamma(2) = (0.8 \pm 0.2)$

→ A power spectral exponent $\beta = \gamma(2) + 1 = (1.8 \pm 0.2)$

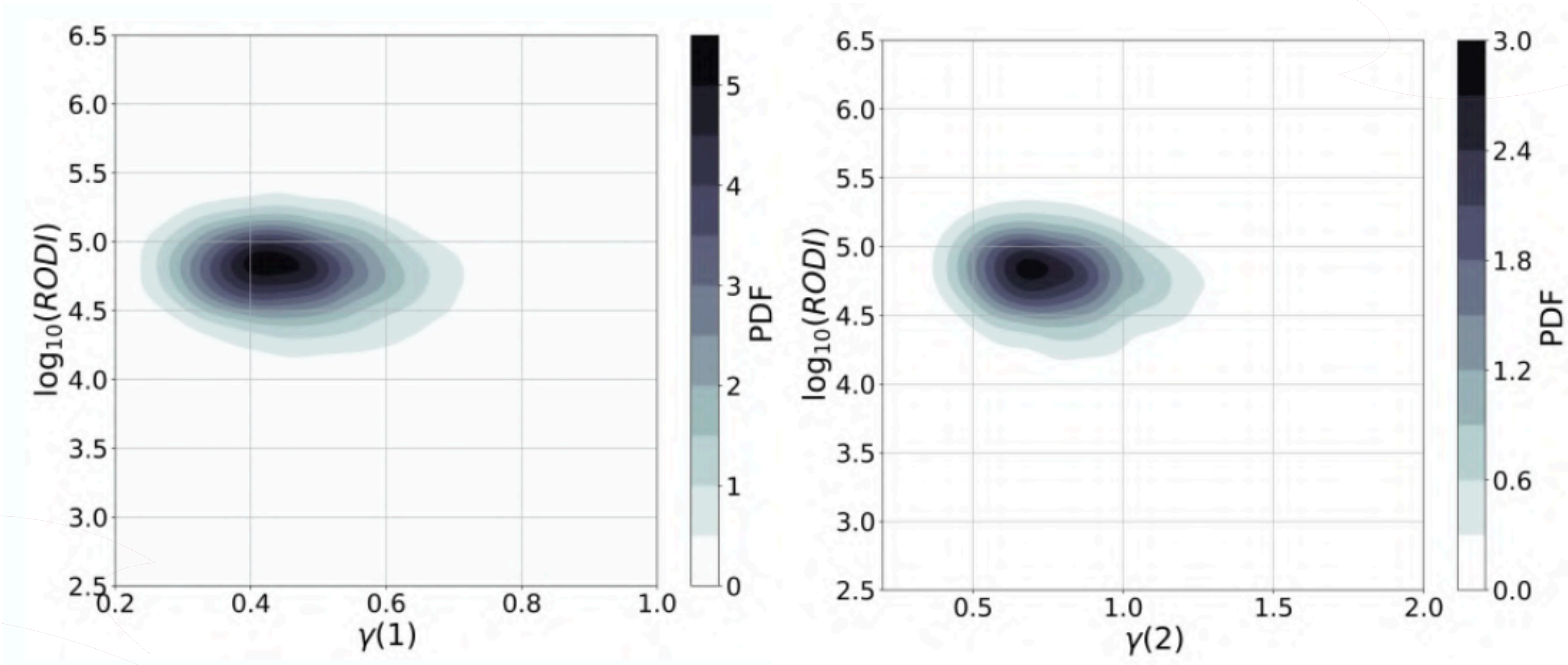

GPS LoL events are mainly associated with $\gamma(1) = (0.47 \pm 0.12)$

Results: Mid and High Latitude (QDLat>50°)

GPS LoL events are mainly associated with $\gamma(2) = (0.8 \pm 0.2)$

→ A power spectral exponent $\beta = \gamma(2) + 1 = (1.8 \pm 0.2)$

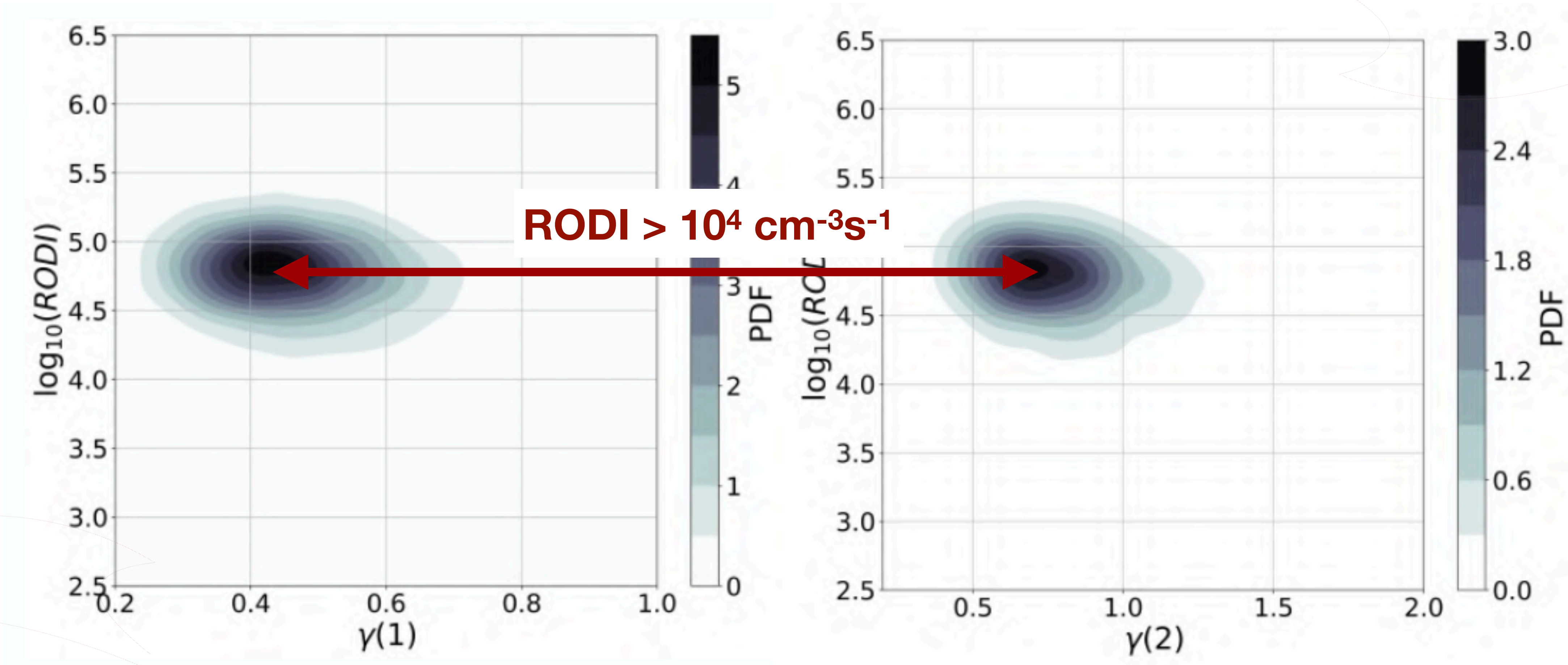

GPS LoL events are mainly associated with $\gamma(1) = (0.47 \pm 0.12)$

Results: Mid and High Latitude (QDLat>50°)

To better characterize this class of events we introduce a pseudo-intermittency

$$\mu = \gamma(1) - 2\gamma(2)$$

It is a measure of how the scaling exponents depart from a linear dependence of the moment order q.

- $\mu > 0$ is exactly what is observed for the occurrence of intermittency in turbulence.
- The greater the value of μ, the greater the non-homogeneity with which the energy is redistributed at all the time and/or spatial scales

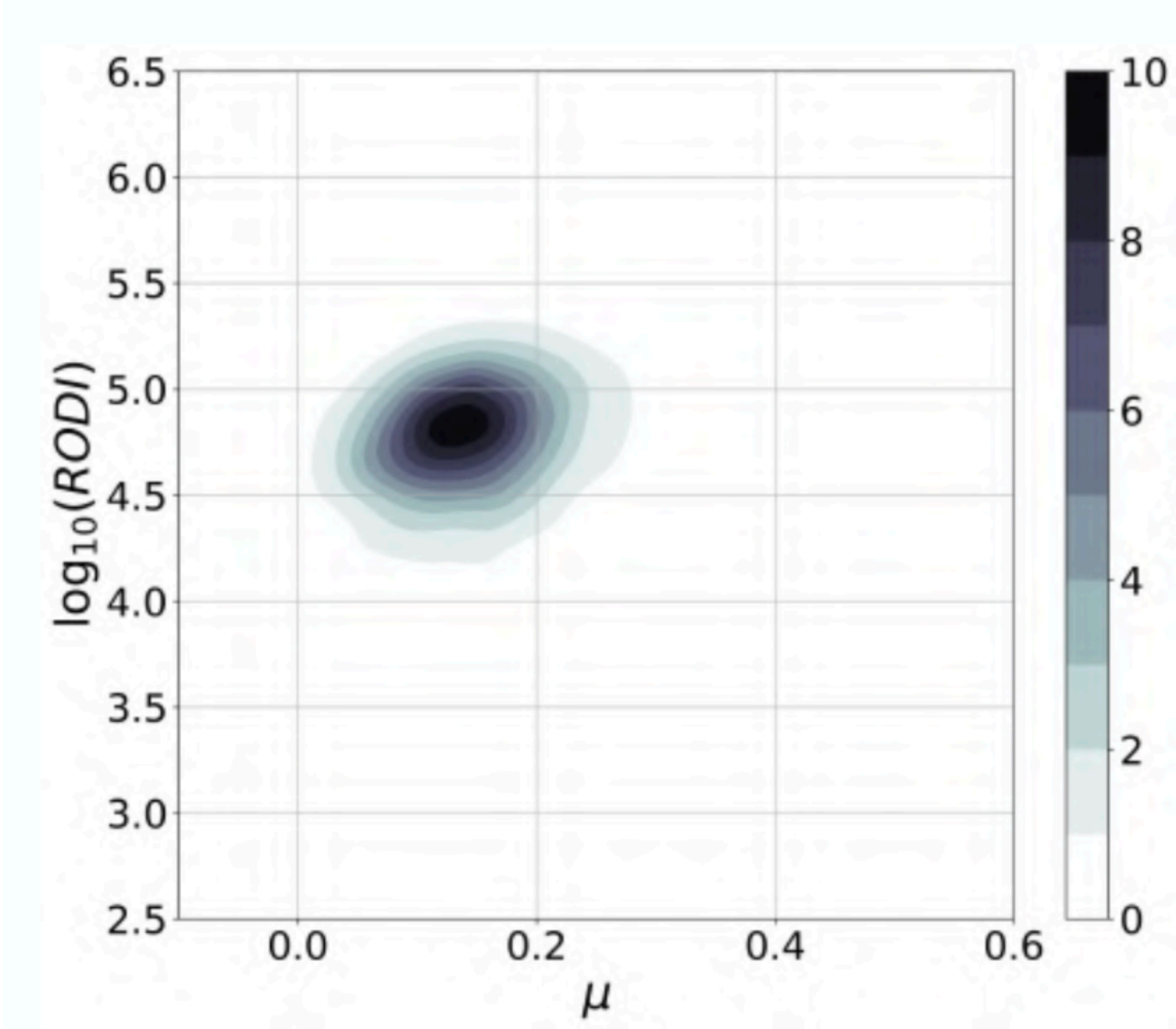

The plasma density irregularities associated with GPS LoL events are in a turbulent state characterized by a certain degree of intermittency.

Results: Mid and High Latitude (QDLat>50°)

The occurrence of GPS LoL events is associated with the specific class of Ne fluctuations. In addition RODI seems to be a proxy of this class: values of Log (RODI) >4 are associated with the occurrence of LoL events

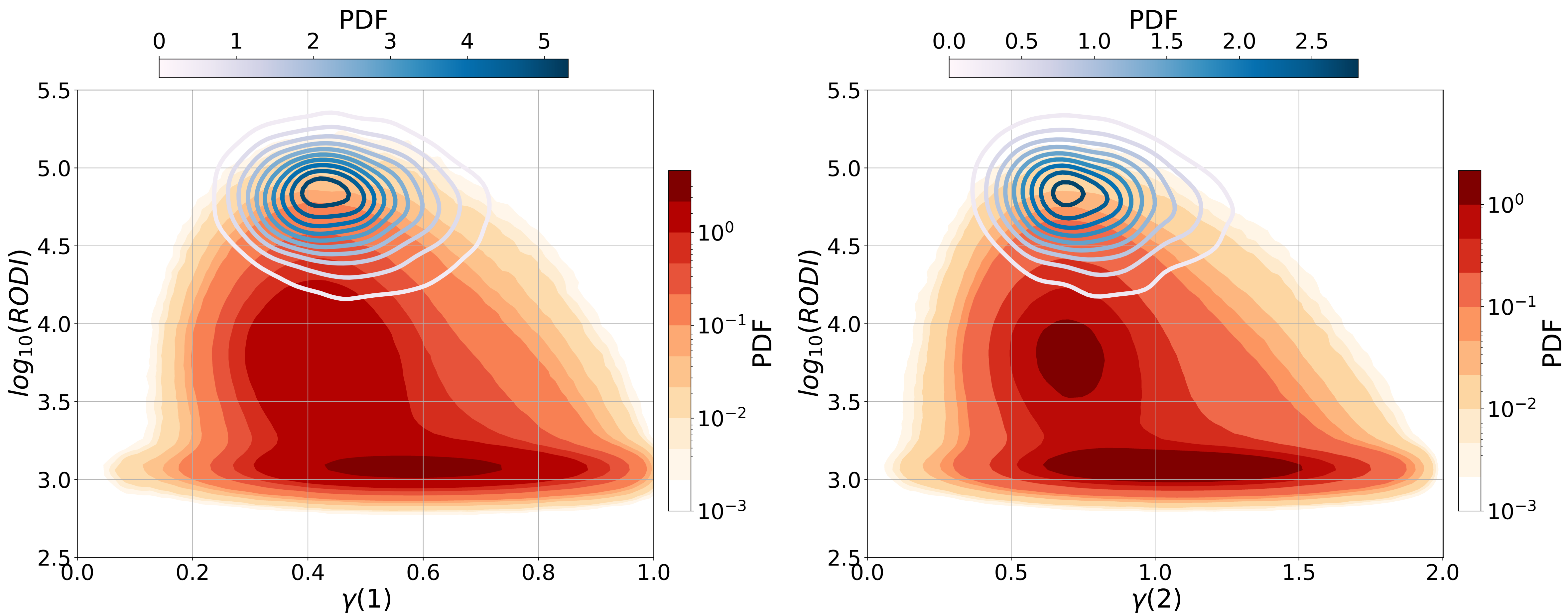

Comparison between the features of Ne fluctuations corresponding to the GPS LoL events and those obtained by considering all the available Ne data recorded in the same regions and for the same period.

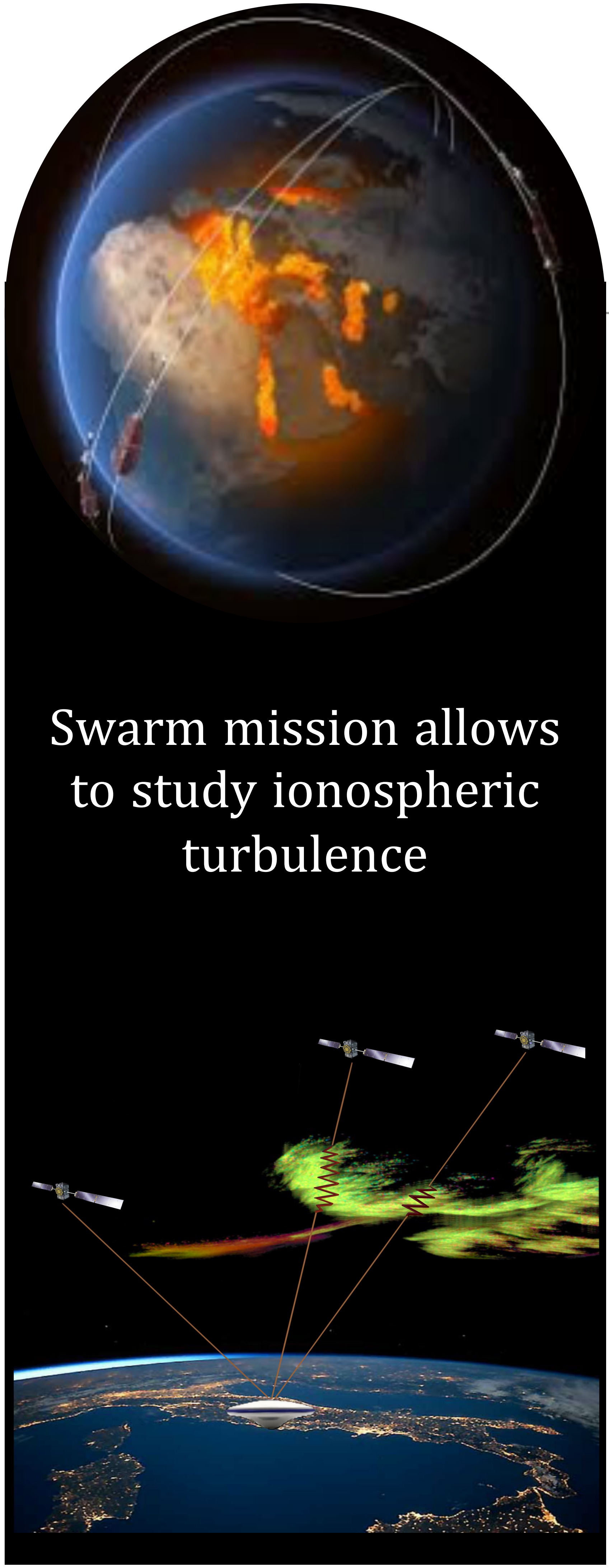

Conclusions

1. There are **two different families of Ne fluctuations** which are characterized by different mean values of scaling exponent and RODI. This finding suggests that two main different classes of physical phenomena can be at the origin of the different scaling features;

2. A population is characterized by antipersistency, $\gamma(2) < 1$ and high values of RODI. This family is mainly located inside the auroral oval, where particle precipitation dominates;

3.The other population is characterized by persistency, $\gamma(2) > 1$ and low values of RODI. It is mainly is located at low latitudes, mainly and outside the auroral oval;

4.The RODI values reasonably capable of capturing the Ne irregularities due to turbulent processes are such that Log(RODI)>3.25 at mid/high latitude, and it is independently on geomagnetic activity level;

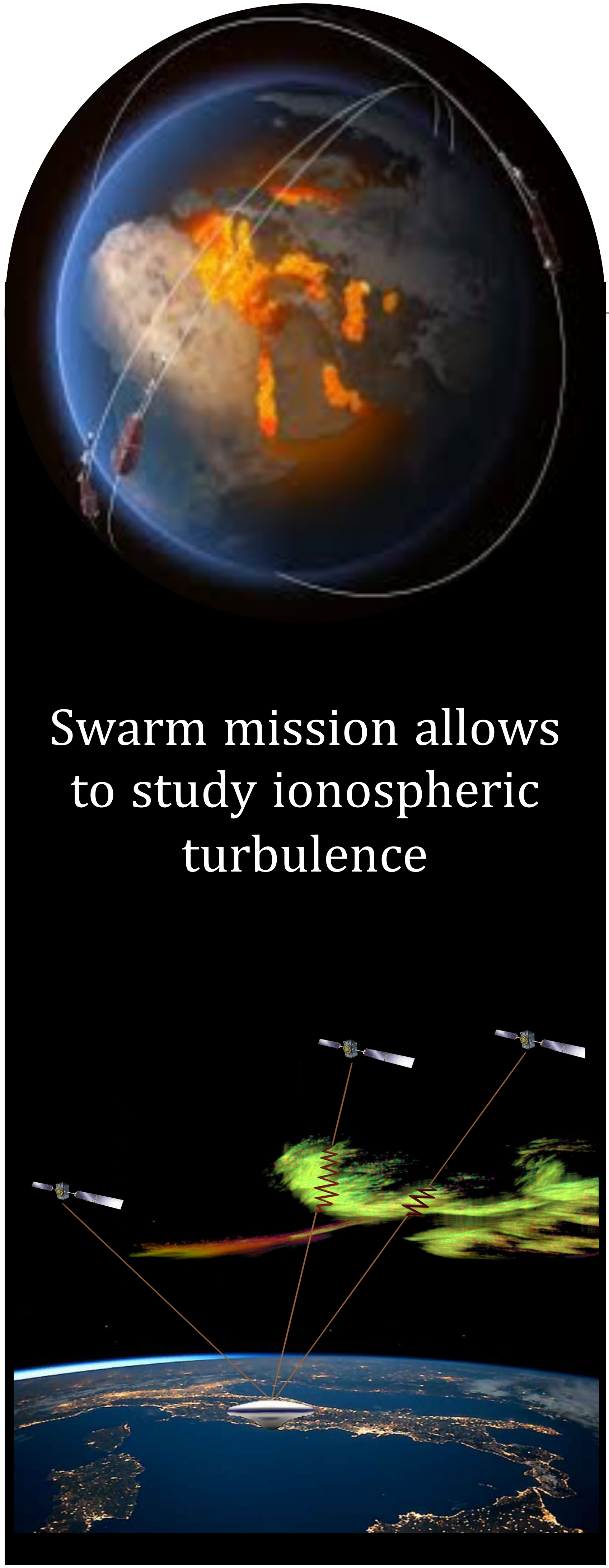

Conclusions

5. The occurrence of **GPS LoL events** is associated with the specific class of Ne fluctuations. When a GPS LoL event is ongoing, Ne fluctuations are in a **turbulent state** characterized by i**ntermittent structures** and generally accompanied by extremely **high values of RODI**.

6. The obtained scaling exponent values are compatible with some processes that generally occur at high latitudes as the **gradient-drift/current convective instability** and the **Kelvin-Helmholtz instability**. These processes are capable of generating turbulence spectra characterized by spectral exponent near -5/3 in the case of direct and inverse cascade.

Papers Published 2020-2022

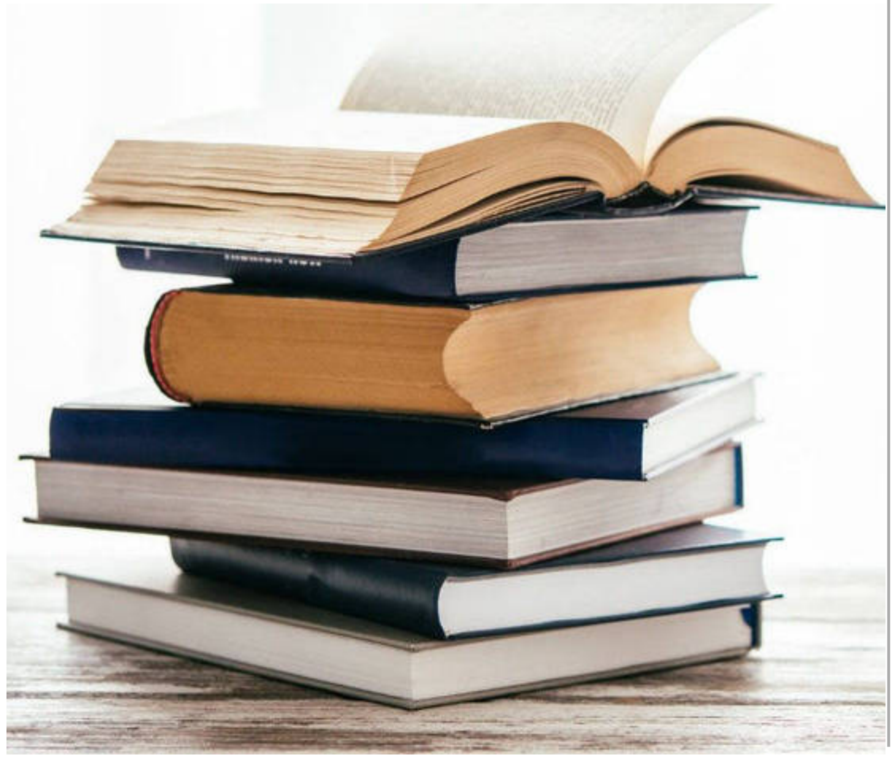

1. De Michelis P., et al., **Journal of Geophysical Research: Space Physics**, 125, e2020JA027934, https://doi.org/10.1029/2020JA027934, 2020

2. Consolini G., et al., **Journal of Atmospheric and Solar-Terrestrial Physics**, 217 https://doi.org/10.1016/j.jastp.2020.105531, 2021.

3. De Michelis P. et al., **Remote Sensing**, 13, 759, https://doi.org/10.3390/rs13040759, 2021.

4. De Michelis P. et al., **Scientific Reports**, 11 https://doi.org/10.1038/s41598-021-84985-1, 2021.

5. Pezzopane M.,et al., **Remote Sensing**, 13, 2209, https://doi.org/10.3390/rs13112209, 2021.

6. De Michelis P., **Remote Sensing**, 14, 918. https://doi.org/10.3390/rs1404091, 2022.